QSP I-O & ADCs: Integration of an antibody-drug conjugates mechanistic model into an immuno-oncology quantitative systems pharmacology platform

Yafei Wang[1], Kyoichi Ebata[2], Tarek Leil[1], Yougan Cheng[1]
1. Daiichi Sankyo Inc., Basking Ridge, NJ 07920, USA; 2. Daiichi Sankyo Co., Ltd., 1-2-58, Hiromachi, Shinagawa-ku, Tokyo 140-8710, Japan

ABSTRACT

Cancer is a complex and dynamic disease characterized by intricate interactions between tumor cells and various other cell types—particularly immune cells—within the tumor microenvironment (TME). Effective treatment remains challenging due to limitations in drug delivery and the evolutionary nature of tumor cell drug resistance, wherein cells acquire mutations or rewire biological pathways to evade therapeutic agents.

Antibody-drug conjugates (ADCs) have emerged as a promising modality in oncology, offering targeted delivery of cytotoxic payloads via the specificity of monoclonal antibodies. To overcome drug resistance and mitigate off-target toxicity, ADCs are increasingly being combined with complementary therapies such as immune checkpoint inhibitors, chemotherapy, and small-molecule inhibitors [1].

In this work, we introduce a Quantitative Systems Pharmacology (QSP) platform for immuno-oncology (I-O) and ADCs. This virtual modeling framework simulates tumor growth dynamics and treatment responses to ADC monotherapy and combination regimens involving I-O agents (e.g., checkpoint inhibitors) and chemotherapy. The I-O QSP platform captures physiological tumor progression and immune cell interactions within a chemokine- and cytokine-rich TME, structured around the cancer-immunity cycle and its subcycles [2]. It also incorporates mechanistic representations of key immuno-oncology interventions, including anti-PD1/PDL1, anti-LAG3, anti-TGFβ, and anti-CTLA4 therapies.

The integrated ADC module models the pharmacokinetics for both antibody and payload components, as well as antigen expression, target engagement, and molecular interactions across plasma, peripheral tissues, and the TME.

The QSP I-O & ADCs platform provides a robust in silico environment for simulating complex tumor dynamics under various therapeutic interventions. It enables strategic optimization of combination therapies and supports rational design of clinical trials.

OBJECTIVE

Antibody-drug conjugates (ADCs) synergize targeted chemotherapy with monoclonal antibody precision, while immuno-oncology (I-O) therapies harness the immune system to combat cancer. Combining these modalities holds promise for overcoming resistance and enhancing therapeutic efficacy in oncology [3]. However, optimizing such combinations can be facilitated by a mechanistic model to predict pharmacokinetic-pharmacodynamic (PK-PD) interactions. In this work, we integrate a mechanistic ADC model into an I-O quantitative systems pharmacology (QSP) platform and aim to design virtual clinical trials for ADC/I-O combination therapies.

WHY IS THIS TOPIC IMPORTANT?

Combination therapies offer several potential advantages over monotherapy, including enhanced efficacy, reduced resistance, synergistic effects, and the potential for personalized treatment strategies. A notable example is the combination of ADCs with immunotherapy, which has emerged as a promising approach in cancer treatment [4].

Immunotherapeutic agents, particularly immune checkpoint inhibitors (ICIs), are effective in stimulating anti-tumor immune responses. However, their clinical application can be limited by challenges such as low response rates in certain patient populations, difficulties in measuring efficacy endpoints, and the occurrence of immune-related adverse events [5].

The combination of ADCs and ICIs leverages complementary mechanisms of action—ADCs deliver cytotoxic payloads directly to tumor cells, while ICIs activate immune effector functions—resulting in a multifaceted therapeutic effect. This dual approach not only enhances anti-tumor activity but also holds potential for overcoming tumor heterogeneity.

Figure 1 illustrates the pharmacodynamic interplay between ADCs and ICIs, highlighting how their combined effects can modulate the tumor microenvironment and improve therapeutic outcomes [3].

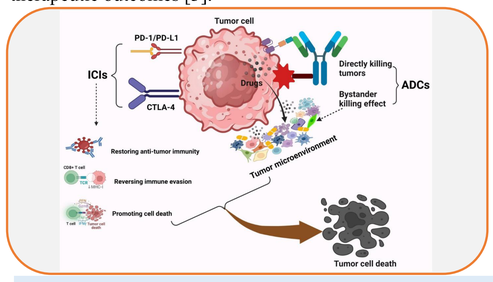

Figure 1: Schematic diagram of combing of ICIs and ADCs
The diagram illustrates the enhanced therapeutic efficacy of combining ICIs and ADCs in cancer therapy. ICIs boost the immune system's ability to target and kill tumor cells, while ADCs deliver cytotoxic agents directly to tumor cells.

Quantitative Systems Pharmacology (QSP) modeling offers transformative advantages for optimizing cancer combination therapies by enabling simulation of complex biological interactions and virtual testing of therapeutic strategies. Rather than relying solely on empirical "trial-and-error" approaches, QSP provides a mechanistic, quantitative, and systems-level understanding of drug actions within the human biological context. Key benefits include:

- Prediction of synergistic effects in drug combinations [6]
- Optimization of dosing and scheduling to maximize efficacy and minimize toxicity [6]
- Incorporation of tumor and patient heterogeneity to support personalized medicine [7]
- Evaluation of resistance mechanisms and exploration of counterstrategies [8]
- Exploration of predictive biomarkers to guide patient selection and stratification [9]
- Acceleration of drug development timelines and reduction of associated costs [10]

METHODS

A mechanistic ADC module was developed, incorporating physiologically based pharmacokinetic models for ADC components (antibody and payload), and soluble antigen and antibody-molecule interaction dynamics across plasma, peripheral tissues, and the tumor microenvironment (TME). The module simulates antibody-antigen monovalent and bivalent binding, internalization, intracellular payload cleavage, payload and intracellular target binding, and cancer cell death in the TME. Two drug-to-antibody ratio (DAR) models were implemented: (i) an individual DAR model, tracking payload deconjugation kinetics across ADC variants [11], and (ii) an analytically derived average DAR model to simplify computational complexity. Both models were embedded into an I-O QSP platform, which models the cancer-immunity cycle and the TME cancer immunity subcycle [2], and immune checkpoint interactions. This model platform integration allows simulation of ADC monotherapy and combination regimens with I-O agents (e.g., checkpoint inhibitors).

I-O QSP framework

Figure 2 (A) shows overview of I-O QSP platform (e.g., compartments, distributions); (B) shows the schematic diagram of the TME compartment as modeled in the I-O QSP disease platform. Within this framework, cancer cells are eliminated through immune-mediated mechanisms and chemotherapy. Tumor-derived debris activates antigen-presenting cells (APCs), which then migrate to the lymph nodes to initiate T cell activation. These activated T cells subsequently return to the tumor site to execute targeted cytotoxic responses against cancer cells.

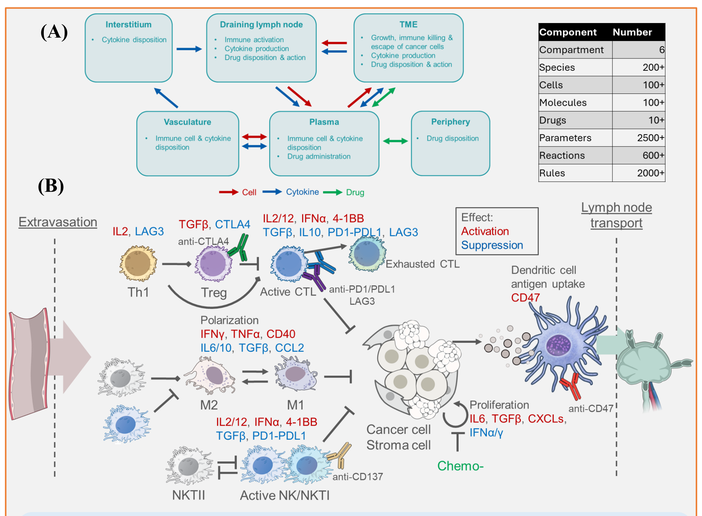

Component	Number
Compartment	6
Species	200+
Cells	100+
Molecules	100+
Drugs	10+
Parameters	2500+
Reactions	600+
Rules	2000+

Figure 2: Diagrams illustrating overview of I-O platform and key interactions within the TME
This figure depicts A) overview of the I-O platform and (B) the interaction dynamics between cancer cells and immune cells, as well as the mechanisms of anti-cancer treatments such as ICIs and chemotherapy.

Integration of ADC model

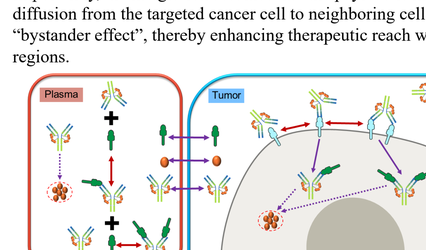

Figure 3: Compartment-Level Model and ADC Pharmacodynamic Effects
This figure illustrates the compartment-level model of ADC and its pharmacodynamic effects. The overall cell-killing impact results from both ADC activity and the natural immune response, such as that from CD8+ T cells.

A mechanistic ADC module was developed and integrated into the I-O QSP platform. Figure 3 and Figure 4 show the schematic diagram of ADC PD in TME and the detailed PK dynamics of ADC components.

The model captures key molecular interactions, including specific binding between antibodies and both soluble and membrane-bound antigens, as well as the binding of deconjugated payloads to intracellular targets. Formation of the payload-target complex initiates cytotoxic activity, leading to cancer cell death.

Importantly, the integration assumes that the payload is membrane-permeable, enabling diffusion from the targeted cancer cell to neighboring cells. This mechanism induces a "bystander effect", thereby enhancing therapeutic reach within heterogeneous tumor regions.

Figure 4: ADC Pharmacokinetics and Mechanism of Action Diagram
This figure illustrates the pharmacokinetic behavior of ADCs within plasma, peripheral tissues, and the tumor microenvironment (TME). It also depicts the interactions between the ADC, antigen, and target-payload.

Two drug-to-antibody ratio (DAR) models

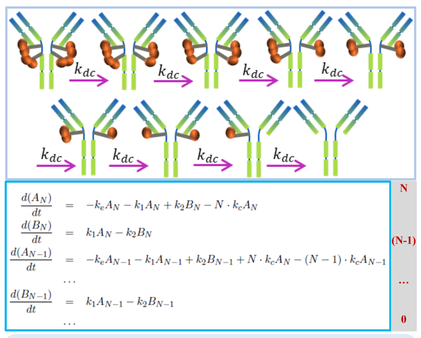

Figure 5: Diagram of the Individual DAR Model
This figure illustrates the kinetics of ADCs and the process of payload deconjugation.

We developed a sequential payload deconjugation model to describe the pharmacokinetics of ADCs in plasma and the dynamics of payload release within the intracellular tumor microenvironment (TME). The model assumes a consistent deconjugation rate across all ADC states, ranging from fully conjugated (N payloads) to completely deconjugated (0 payload). While this is a generalized approach, the actual process could be more complex depending on the specific ADCs and payload types involved. Adjustments or enhancements to the deconjugation parameters can be made as needed.

We subsequently integrated an additional payload deconjugation model, referred to as the "Average Drug-to-Antibody Ratio (DAR)" model. Figure 6 illustrates the underlying assumptions and the model schematic. In this framework, the total amount of ADCs across plasma and peripheral compartments—and consequently the total payload—is computed as the sum of conjugated payloads multiplied by the respective quantities of each ADC state.

Through analytical derivation, we demonstrated that the kinetics of total ADCs and payload are independent of the distribution across individual ADC states. It is important to note that this result is contingent upon the assumption of a uniform payload deconjugation rate across all ADC species.

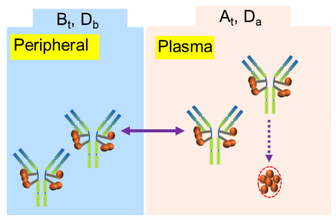

$$A_t = A_0 + A_1 + \ldots + A_N$$
$$B_t = B_0 + B_1 + \ldots + B_N$$
$$D_a \cdot A_t = 0 \cdot A_0 + 1 \cdot A_1 + \ldots + N \cdot A_N$$
$$D_b \cdot B_t = 0 \cdot B_0 + 1 \cdot B_1 + \ldots + N \cdot B_N$$

Figure 6: Diagram of the Average DAR Model
This figure illustrates the average DAR model kinetics for payload deconjugation from ADC.

RESULTS

The integrated individual DAR model (IDM) accurately represented the physiological distribution of various ADC states, soluble antigens, and payloads within plasma and the TME, both extracellularly and intracellularly. Comparative analysis revealed that the average DAR model (ADM) recapitulates key outcomes of the individual DAR model—such as plasma ADCs/payload levels, intracellular payload concentrations, and tumor growth dynamics—with high fidelity under physiological conditions. This parity suggests the average DAR model can simplify ADC QSP workflows without compromising accuracy. Furthermore, the platform considered immune modulation in the TME during ADC/I-O combination therapy, highlighting synergies between payload-induced immunogenic cell death and immune activation.

ADC states dynamics

Figure 7 presents the simulation results of bivalent binding dynamics for antibody-drug conjugates within the IDM framework across different compartments. In this demonstration, each ADC molecule carries 8 payloads, resulting in a total of 9 distinct conjugation states. The distribution of these individual states is governed by the payload deconjugation kinetics and evolves over time.

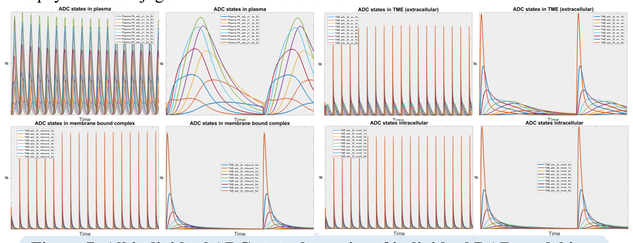

Figure 7: All individual ADC state dynamics of individual DAR model in plasma and TME
The figure shows various bivalent binding ADC dynamics of IDM in plasma and TME. (Left: all duration time, Right: ~ 1 cycle time of left figure.

Figure 8 shows the comparison results of total bivalent binding ADC of IDM (which is corresponding to results of Figure 7) and ADM. As mentioned in the method section of average DAR model, we defined--the ADC state of ADM is equal to total of various ADC states in plasma and peripheral compartments. Therefore, the simulations of analytical derivation should be consistent with our prior assumption. Figure 8 demonstrates the consistent simulation results of IDM and ADM, which is subject to our prior method assumptions.

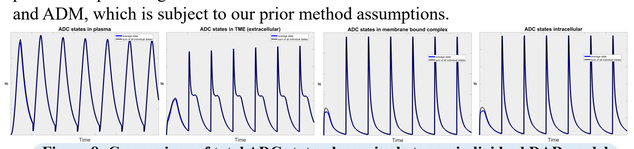

Figure 8: Comparison of total ADC states dynamics between individual DAR model and average DAR model
This figure presents a summary of different bivalent binding ADC states dynamics of IDM compared to the corresponding total ADCs of ADM in both plasma and the tumor microenvironment (TME).

Payload dynamics in plasma and TME

Figure 9 compares payload concentrations between IDM and ADM in plasma and TME. As described in the methods section, the DAR release process was modeled using a sequential payload deconjugation approach. The analytical derivation of the average DAR model is independent of individual ADC states.

Simulation results show that ADM effectively recapitulates the payload levels observed in IDM across compartments. This approach significantly simplifies model implementation, especially for ADCs with high DAR values.

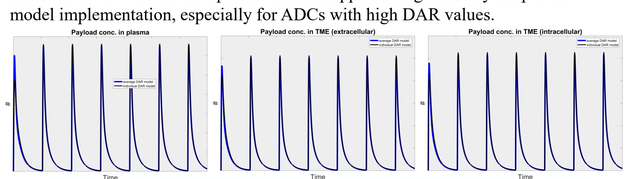

Figure 9: Comparison of Payload Concentration Dynamics Between Individual DAR Model and Average DAR Model
This figure presents simulation outcomes illustrating the payload concentration in plasma and the tumor microenvironment (TME) for both the Individual DAR Model (IDM) and the Average DAR Model (ADM).

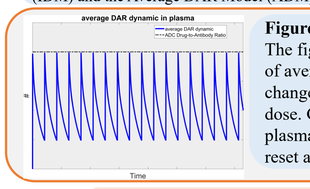

Figure 10: average DAR dynamics
The figure demonstrates the simulation result of average DAR dynamics. It periodically changes which corresponds the administration dose. Given large injection dose amount (in plasma) compared with TME, average DAR is reset almost the original DAR ratio.

Antigen, target and tumor dynamics

Figure 11 shows simulation results for soluble antigen, target, and target-payload complex in plasma and TME across two DAR models. In the MoA of this demo ADC, the intracellular payload binds to its target molecule, forming a payload-target complex. Upon cancer cell apoptosis, membrane antigen, target, and target-payload complex can be released into the extracellular TME. The results demonstrate consistent behavior between the two DAR models, supporting the robustness of the implementation.

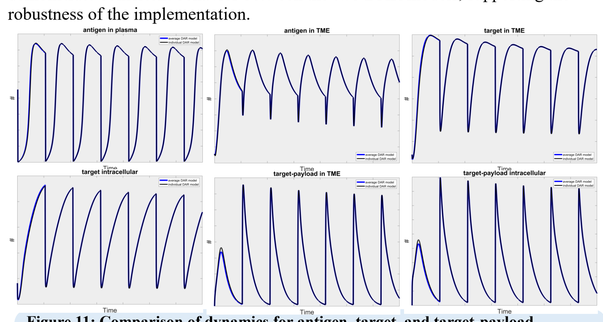

Figure 11: Comparison of dynamics for antigen, target, and target-payload complexes in individual and average DAR models
This figure presents simulation outcomes for soluble antigen, target, and the payload-target complex.

To model the molecular-level binding kinetics of ADC-antigen and payload-target interactions, we explicitly defined ODEs for all molecular species based on their amounts. This means that the quantities of membrane antigen and intracellular target are proportionally linked to cancer cell dynamics. Figure 12 demonstrates mass balance for membrane antigen and intracellular target, showing consistent behavior across both DAR models.
Figure 13 provides example results of cell- and tumor-level dynamics under the two DAR models. In our platform, tumor volume is composed of the volumes of various cell types (e.g., cancer cells, stroma, Tregs), as well as extracellular, vascular, and interstitial spaces. From the calculated tumor volume, lesion-level metrics such as SLD and relative SLD change can be derived—useful for classifying clinical response rates.

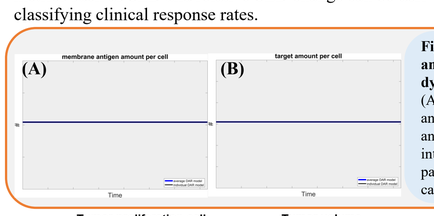

Figure 12: Membrane antigen and target mass balance dynamics
(A) indicates the membrane antigen amount per cancer cell and (B) represents the intracellular target (and target-payload complex) amount per cancer cell.

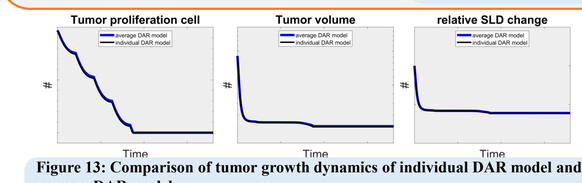

Figure 13: Comparison of tumor growth dynamics of individual DAR model and average DAR model
The figure represents cancer cell population, tumor volume and relative sum of longest diameter (SLD) change dynamics.

CONCLUSIONS

By integrating ADC mechanistic modeling with an I-O QSP platform, this work establishes a versatile platform for virtual clinical trial design. Future studies will explore extracellular payload release, immunomodulatory effects of ADCs [12], and patient-specific virtual cohort calibration for indications such as breast or lung cancer. It also can be adapted to model specific permeability of payloads and new MoAs of payloads for ADCs. The platform's capability to simulate combination therapies could help streamline early clinical development, reduce trial costs, and identify optimal dosing regimens.

Virtual population

In the simulation results of the integrated QSP I-O & ADCs platform, a single parameter set—representing one virtual patient—was used for demonstration purposes. To support clinical trial design, it is essential to develop a virtual population that captures physiological and disease variability. This enables modeling of inter-individual differences in patient responses and calibration against observed clinical variability [11].

Such a framework allows for prediction of outcomes across diverse patient subgroups, particularly in scenarios where clinical data is limited or complex. Figure 14 illustrates example sampling outcomes generated by the integrated QSP platform.

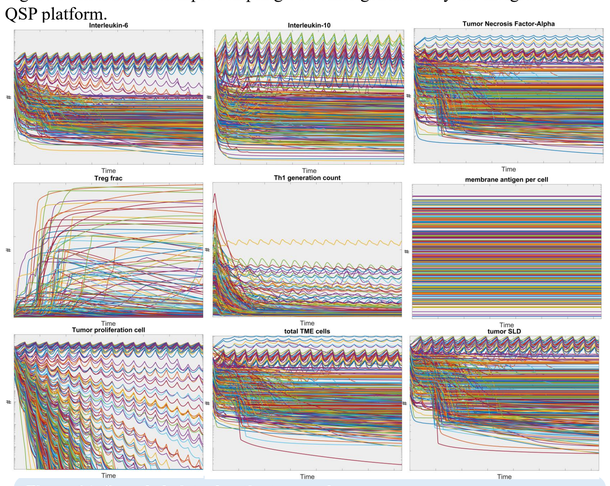

Figure 14: Sampled virtual patient examples
This figure illustrates sample simulation results across various molecule, cell and tumor scales, generated by selecting particular parameter configurations.

ADCC/ADCP induced by conjugated antibody

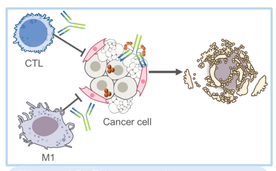

Figure 15: Diagram of ADCC/ADCP by conjugated antibody. The figure shows the conjugated antibody of ADCs may also induce additional effects.

In the demo simulation of this platform, we assumed that the conjugated antibody component of ADCs serves solely as a delivery vehicle for the payload, without contributing directly to cancer cell killing. However, recent studies suggest that the antibody backbone of ADCs can engage Fcγ-receptors and trigger antibody-dependent cellular phagocytosis (ADCP) [12]. This is plausible, given that many antibodies used in ADCs possess inherent immune-stimulatory properties. Functionally, this resembles a combination therapy involving both payload-driven ADCs and ICIs.

Permeable payload vs non-permeable payload

In the demo simulation of this platform, we assumed that payload is permeable. That means the extracellular payload (e.g., flux from plasma, released from cancer cell apoptosis which contains internalized ADCs) can enter surrounding cancer cells and kill them.
This strategy enhances the overall efficacy of the ADCs, especially in tumors with heterogeneous antigen expression, by creating a broader anti-cancer effect. However, this permeability also requires careful balancing, as it can contribute to off-target toxicity if the payload leaks into non-cancerous cells. Therefore, dose optimization is important.

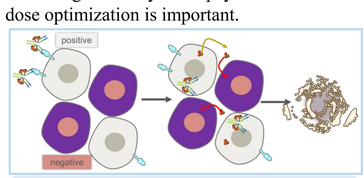

Figure 16: Permeable payload induces bystander effect. Permeable payload can induce death of surrounding antigen-negative cancer cells.

Some ADCs may use non-permeable payload. This limits the bystander effect, but makes it ideal for targeting antigens with high expression to minimize off-target toxicity. In the platform, modeling payload-specific permeability is straightforward and can be achieved by adjusting the relevant permeation parameters.

New MoAs of payloads for ADCs

In the demo simulation of this platform, the MoAs of payload is to bind with intracellular target and format payload-target complex, increasing cancer cell apoptosis rate. New types of payloads for ADCs include immune-modulating agents (like TLR agonists), radiometals for therapy, RNA inhibitors, protein degraders, and the incorporation of multiple diverse payloads. This significantly increases model complexity as it triggers other type of cells and especially for immunity systems (e.g., Figure 17). It requires complex mechanism driven model platform for capturing the specific MoAs of payloads.

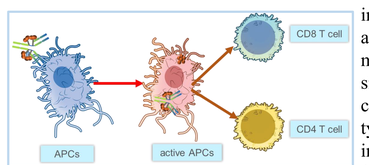

Figure 17: Immune-modulating ADCs
The figure shows the immune-modulating ADCs can activate APCs and then improve T cell activation.

ACKNOWLEDGEMENT

- We acknowledge Daiichi Sankyo's funding support for working on this project.
- We also appreciate Daiichi Sankyo's model development team (MDT) for providing feedbacks on this platform.
- All authors are employees of Daiichi Sankyo. Y. W., T. L. and Y. C. are also shareholders of Daiichi Sankyo.

REFERENCES

[1] S., X. et al., Front. Pharmacol. 16, 1556245 (2025). DOI: 10.3389/fphar.2025.1556245
[2] M., I., et al., Immunity 56, 2188 (2023). DOI: 10.1016/j.immuni.2023.09.011
[3] Y., P., et al., Cell Death Dis 15, 433 (2024). DOI: 10.1038/s41419-024-06837-w
[4] A., F., J., et al., Trends in Cancer 9, 339 (2023). DOI: 10.1016/j.trecan.2023.01.003
[5] M., D., M., et al., Cancer Cell 38, 326 (2020). DOI: 10.1016/j.ccell.2020.07.004
[6] L., Y., et al., npj systems biology and applications 11, 63 (2025). DOI: 10.1038/s41540-025-00544-8
[7] A., T., et al., Science Advances 9, 26 (2023). DOI: 10.1126/sciadv.adg0289
[8] Z., Y., et al., Acta Pharmacol Sin. 45, 1287 (2024). DOI: 10.1038/s41401-024-01232-9
[9] M., O., et al., Scientific Reports 9, 11286 (2019). DOI: 10.1038/s41598-019-47802-4
[10] S., C., L., J. Pharmacokinet Pharmacodyn 51 551 (2024). DOI: 10.1007/s10928-024-09905-y
[11] C., Y., et al., AAPS J 19, 1002 (2017). DOI: 10.1208/s12248-017-0100-x
[12] T., L., et al., Nat Commun 16, 3167 (2025). DOI: 10.1038/s41467-025-58266-8